

# Near-Infrared Super-Absorbing All-Dielectric Metasurface Based on Single-Layer Germanium Nanostructures

Jingyi Tian, Hao Luo, Qiang Li,\* Xuelu Pei, Kaikai Du, and Min Qiu

**Strong near-infrared absorption in ultrathin semiconductor layers is essential for increasing the speed and efficiency of photocarrier extraction in optoelectronic devices. However, the absorption of a free-standing ultrathin film can never exceed 50% in principle. In this article, an all-dielectric germanium metasurface absorber in the near-infrared region (800–1600 nm) is proposed theoretically and experimentally. Near-unity absorption can be achieved in such a subwavelength-thin ( $\approx 0.13 \lambda_0$ ) layer of nanostructures based on the destructive interference between simultaneously excited electric and magnetic dipoles inside each element in the backward direction in combination with the destructive interference between the scattered field and the incident field in the forward direction. Its response is both polarization-independent and angle-insensitive, with over 80% absorption at an incident angle up to  $28^\circ$ . This ultrathin and flexible design paves the way for realizing next generation optoelectronic devices aimed for high-speed photon detection and energy harvesting.**

## 1. Introduction

Near-infrared semiconductor absorbers have attracted growing interest due to their potential applications for realizing highly efficient optoelectronic devices, such as sensors,<sup>[1–3]</sup> photodetectors,<sup>[4–6]</sup> thermophotovoltaic systems.<sup>[7–9]</sup> Especially, strong absorption in optically thin layers is the key to reducing the photocarrier extraction time and enhancing the photocarrier extraction efficiency in optoelectronic devices. As pointed out by Wilhelm Woltersdorff in 1934, the absorption in an ultrathin free-standing film cannot exceed 50%.<sup>[10]</sup> Therefore, in order to achieve high absorption in the semiconductors without the aid of waveguide or multilayer resonators, a thick semiconductor

layer is necessary. For example, traditional p-i-n designs in near-infrared germanium (Ge) photodetectors require an intrinsic Ge layer with a thickness larger than  $1 \mu\text{m}$ .<sup>[6]</sup> The relatively long operating distance hinders the fast response of the devices.

So far, strategies for breaking the 50% absorption limit in the visible and infrared region are mainly based on metal-dielectric<sup>[11–28]</sup> schemes. These strategies include metal–insulator–metal plasmonic absorbers,<sup>[12–21]</sup> dielectric-on-metal absorbers,<sup>[22,23]</sup> film stacks-based Fabry-Perot cavity absorbers,<sup>[24–27]</sup> etc. However, for these designs with the aid of metals, a significant portion of absorption takes place in metals, where heat instead of photocarriers is generated. This is not favorable for developing optoelectronic devices. Besides, the back metallic reflector results in strong reflections

outside the absorption band, which limits the freedom to design a resonant absorber that is transparent out of the absorption band.<sup>[29]</sup> In this circumstance, the concept of all-dielectric metasurfaces<sup>[30–35,41–50]</sup> is adopted to construct all-dielectric absorber without the aid of metals<sup>[36,37]</sup> and it has been experimentally demonstrated in the terahertz region using silicon.<sup>[38,39]</sup>

In this article, we propose a Ge nanoantenna-based all-dielectric metasurface to overcome the 50% absorption limit in the ultrathin semiconductor films in the near-infrared region (800–600 nm). Ge shows a high refractive index over 4.2 and considerable absorption in this range.<sup>[40]</sup> Based on the interference between the simultaneously induced electric dipole and magnetic dipole resonances inside each element of the metasurface along with the interference between the scattered field and incident field, we show both theoretically and experimentally that near-unity absorption can be achieved in subwavelength-thin ( $\approx 0.13 \lambda_0$ ) Ge nanostructures without the aid of back reflector in the near-infrared region (800–1600 nm). The absorption is angle-insensitive as well as polarization-independent, with over 80% absorption within an incident angle up to  $28^\circ$ . This single-layer metasurface absorber holds high promise for various high-speed optoelectronic applications, such as using it as an absorption layer for large-area near-infrared photodetectors. It is also compatible with CMOS technology, which will be beneficial for future monolithic integration.

Dr. J. Tian, Dr. H. Luo, Prof. Q. Li, Dr. X. Pei, Dr. K. Du, Prof. M. Qiu  
State Key Laboratory of Modern Optical Instrumentation  
College of Optical Science and Engineering  
Zhejiang University  
Hangzhou 310027, China  
E-mail: qiangli@zju.edu.cn

J. Tian  
Laser Physics  
Department of Applied Physics  
KTH Royal Institute of Technology  
10691 Stockholm, Sweden

 The ORCID identification number(s) for the author(s) of this article can be found under <https://doi.org/10.1002/lpor.201800076>

DOI: 10.1002/lpor.201800076

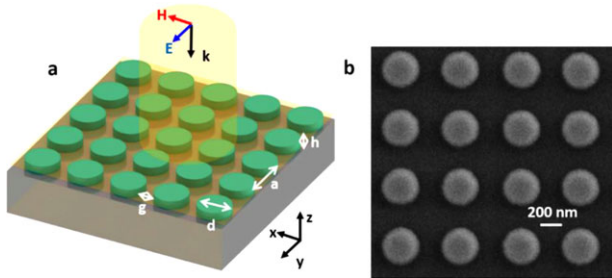


**Figure 1.** a) A schematic and b) an SEM image of the fabricated all-dielectric metasurface absorber with square arrays of Ge disks on a  $\text{CaF}_2$  substrate under the illumination of a  $y$ -polarized near-infrared light, where the height  $h = 160$  nm, gap  $g = 250$  nm, and periodicity  $a = d + g$ .

## 2. Experimental Section

### 2.1. Fabrication of Ge Absorber

A 380 nm-thick PMMA (950K AR-P 672.11) was spun onto  $\text{CaF}_2$  substrate as electron beam resist and baked for 3 min at 150 °C. Then a 50 nm-thick conductive protective coating (AR-PC 5090.02) was spun onto the PMMA film and baked for 2 min at 90 °C. This coating is for the dissipation of e-beam charges on insulating substrates. The PMMA was exposed to define the nanohole array by E-beam lithography. The conductive layer was dissolved in DI water and then the PMMA was developed in 1:3 methyl isobutyl ketone/isopropyl alcohol (IPA) solution followed by rinsing in IPA. After development, a 160 nm-thick Ge film is

then deposited onto the sample by thermal evaporation. The Ge absorber is realized after lift-off by ultrasonic processing in acetone for 1 min.

### 2.2. Optical Measurements

The transmission and reflection spectra under normal incidence are measured by a Fourier transform infrared spectrometer (FTIR) with an InGaAs (D427) detector. Air is used as the reference for measuring the transmittance and a flat gold film deposited onto K9 glass is used as the reference for measuring the reflectance.

### 2.3. Numerical Simulations

Finite-difference time-domain method (FDTD Solutions v8.15, Lumerical) is used to compute the optical responses of single Ge disks and Ge metasurface absorber. The optical constants of Ge are from Palik's handbook.<sup>[40]</sup> The spectral range in the simulation ranges from 800 nm to 1600 nm. The overall structure is illuminated by plane waves propagating along the  $z$ -axis.

## 3. Results and Discussion

To make a trade-off between degrees of freedom of tailoring electromagnetic resonances and the fabrication complexity, we utilize

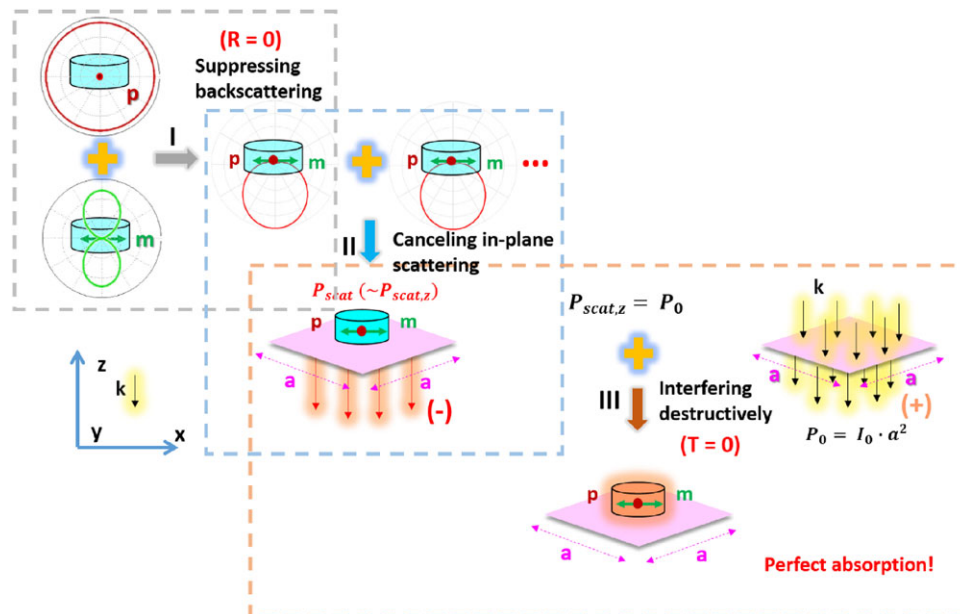


**Figure 2.** The principle of perfect absorption for all-dielectric metasurface absorber consisting of Ge disks with multipolar resonances. I: The interference between the simultaneously induced electric dipole moment ( $p$ ) and magnetic dipole moment ( $m$ ) inside a single Ge disk gives rise to suppressed backward scattering. When forming a metasurface from these Ge disks, there is no backward scattering from each disk, which means there is no reflection ( $R = 0$ ) from this structure. II: When forming a metasurface, the in-plane scattering is canceled due to the destructive interference between adjacent disks in the lateral direction. III: The re-emitted field from each disk is out of phase with the incident one. By adjusting  $a$  to make  $P_{\text{scat},z} = P_0$  for each period, the transmission of the structure can also be suppressed ( $T = 0$ ), where  $P_{\text{scat},z}$  denotes the forward scattered power of an individual disk along  $z$ -direction,  $P_0$  denotes the incident power within each period. Perfect absorption  $A = 1 - R - T = 100\%$  can thus be achieved.

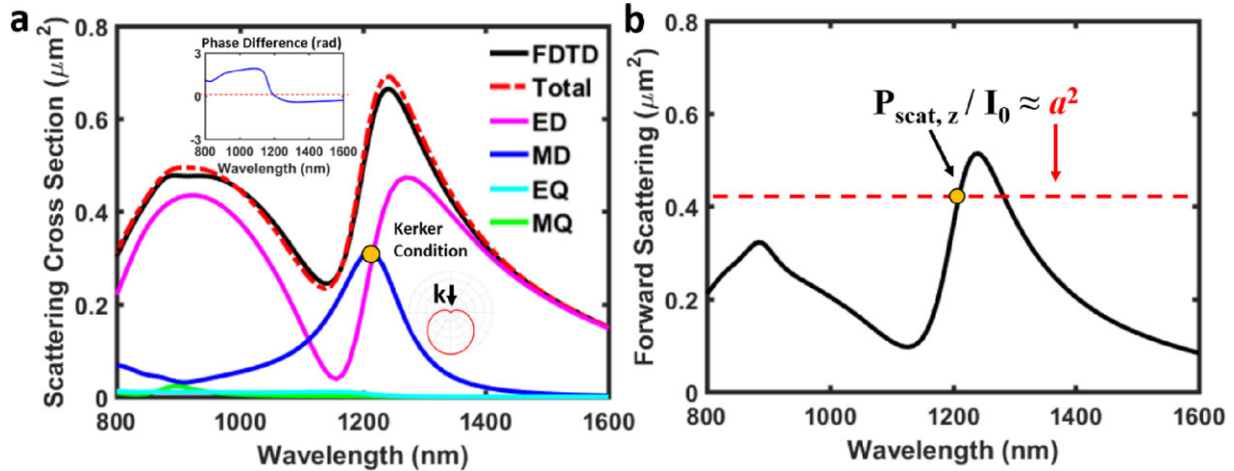


**Figure 3.** a) Scattering properties of a single Ge disk with  $h = 160$  nm and  $d = 400$  nm in vacuum. The total scattering cross section is decomposed into an electric dipole (ED, magenta solid line), a magnetic dipole (MD, blue solid line), an electric quadrupole (EQ, cyan solid line) and a magnetic quadrupole (MQ, green solid line) under the normal incidence of the plane wave. The black solid line represents the result from our FDTD simulation for the total scattering cross-section, while the red dashed line shows the sum of the multipole scattering cross sections. The inset on the upper left shows the phase difference between the induced electric dipole and magnetic dipole. The inset on the lower right shows the radiation pattern of such a disk near the wavelength of 1200 nm. b) Forward scattering cross section of a single Ge disk with  $h = 160$  nm and  $d = 400$  nm in vacuum. The red dashed line represents the desired  $a^2$  to achieve  $T = 0$  for perfect absorption near 1200 nm.

the Ge disk as the element to form square arrays in the metasurface. The metasurface is located on a transparent  $\text{CaF}_2$  substrate ( $n_s = 1.43$ ), as depicted in **Figure 1a**, with the height  $h = 160$  nm and the periodicity  $a = d + g$ , where the gap size  $g = 250$  nm. The corresponding SEM (Scanning Electron Microscope) image of the metasurface is shown in **Figure 1b**.

Achieving perfect absorption in an ultrathin Ge layer is equivalent to simultaneously suppressing its transmission ( $T$ ) and reflection ( $R$ ). Owing to the high refractive index of Ge, the resonant behavior of the single disk is maintained in the metasurface. Therefore, the requirement of perfect absorption can be articulated by the multipolar resonances in each Ge disk, as illustrated in **Figure 2**.

When forming 2D arrays, the individual Ge disk can be represented by a pair of electric ( $\mathbf{p}$ ) and magnetic dipoles ( $\mathbf{m}$ ) along  $y$ -axis and  $x$ -axis, respectively. These dipoles can be characterized by the effective polarizabilities ( $\alpha_{eff}^e$  and  $\alpha_{eff}^m$ ), which show Lorentzian frequency dependence as follows,<sup>[47]</sup>

$$\alpha_{eff}^e = \frac{\alpha_0^e}{\omega_e^2 - \omega^2 - 2i\gamma_e\omega} \quad (1)$$

$$\alpha_{eff}^m = \frac{\alpha_0^m}{\omega_m^2 - \omega^2 - 2i\gamma_m\omega} \quad (2)$$

where  $\alpha_0^e$  and  $\alpha_0^m$  denote the amplitude of the effective polarizabilities.  $\omega_e$  and  $\omega_m$  correspond to the resonance positions and  $\gamma_e$  and  $\gamma_m$  represent damping parameters. The transmission ( $\mathbf{t}$ ) and reflection ( $\mathbf{r}$ ) coefficients of the metasurface can be expressed as,<sup>[47]</sup>

$$\mathbf{t} = 1 + \mathbf{t}_e + \mathbf{t}_m = 1 + \frac{ik_0}{2a^2} (\alpha_{eff}^e + \alpha_{eff}^m) \quad (3)$$

$$\mathbf{r} = \mathbf{r}_e + \mathbf{r}_m = (ik_0)/(2a^2) (\alpha_{eff}^e - \alpha_{eff}^m) \quad (4)$$

where  $\mathbf{k}_0$  is the wave vector in the background medium and  $a$  denotes the period of the metasurface.

First, in order to satisfy the impedance matching condition for zero reflection ( $R = |\mathbf{r}|^2 = 0$ ) for this structure, an electric dipole resonance (ED) and a magnetic dipole resonance (MD) should be induced simultaneously inside each Ge disk. When they spectrally overlap and oscillate in phase with each other, a unidirectional forward scattering behavior instead of a donut-shaped radiation appears, known as Kerker Condition,<sup>[41–46,50]</sup> where  $\alpha_{eff}^e = \alpha_{eff}^m$ . Therefore, there is no re-emission of the electromagnetic field in the backward direction,<sup>[45,46]</sup> that is,  $R = 0$  ( $\mathbf{r} = 0$ ) (**I** in **Figure 2**).

Furthermore, when forming a metasurface with such Ge disks ( $a < \lambda_0/n_s$ ), the in-plane scattering of each disk is canceled and only the scattering into the  $-z$  direction exists due to the destructive interference between the adjacent disks in the lateral direction. (**II** in **Figure 2**).

It is worth noticing that at the crossing of the two resonances ( $\omega = \omega_e = \omega_m = \omega_0$ ), the effective polarizabilities can be correspondingly simplified as

$$\alpha_{eff}^e = i \frac{\alpha_0^e}{2\gamma_e\omega_0} \quad (5)$$

$$\alpha_{eff}^m = i \frac{\alpha_0^m}{2\gamma_m\omega_0} \quad (6)$$

By substituting Equation (5) and Equation (6) into Equation (3), it is obvious that the forward emission of the electric dipole ( $\mathbf{t}_e < 0$ ) is out of phase with the incident field. The same condition applies to the forward emission of the magnetic dipole ( $\mathbf{t}_m < 0$ ). Therefore, we can conclude that the scattered field from the metasurface interferes destructively with the incident field in the forward direction.<sup>[44,47]</sup> Then, in order to cancel the emission from the structure with the incident wave in the forward

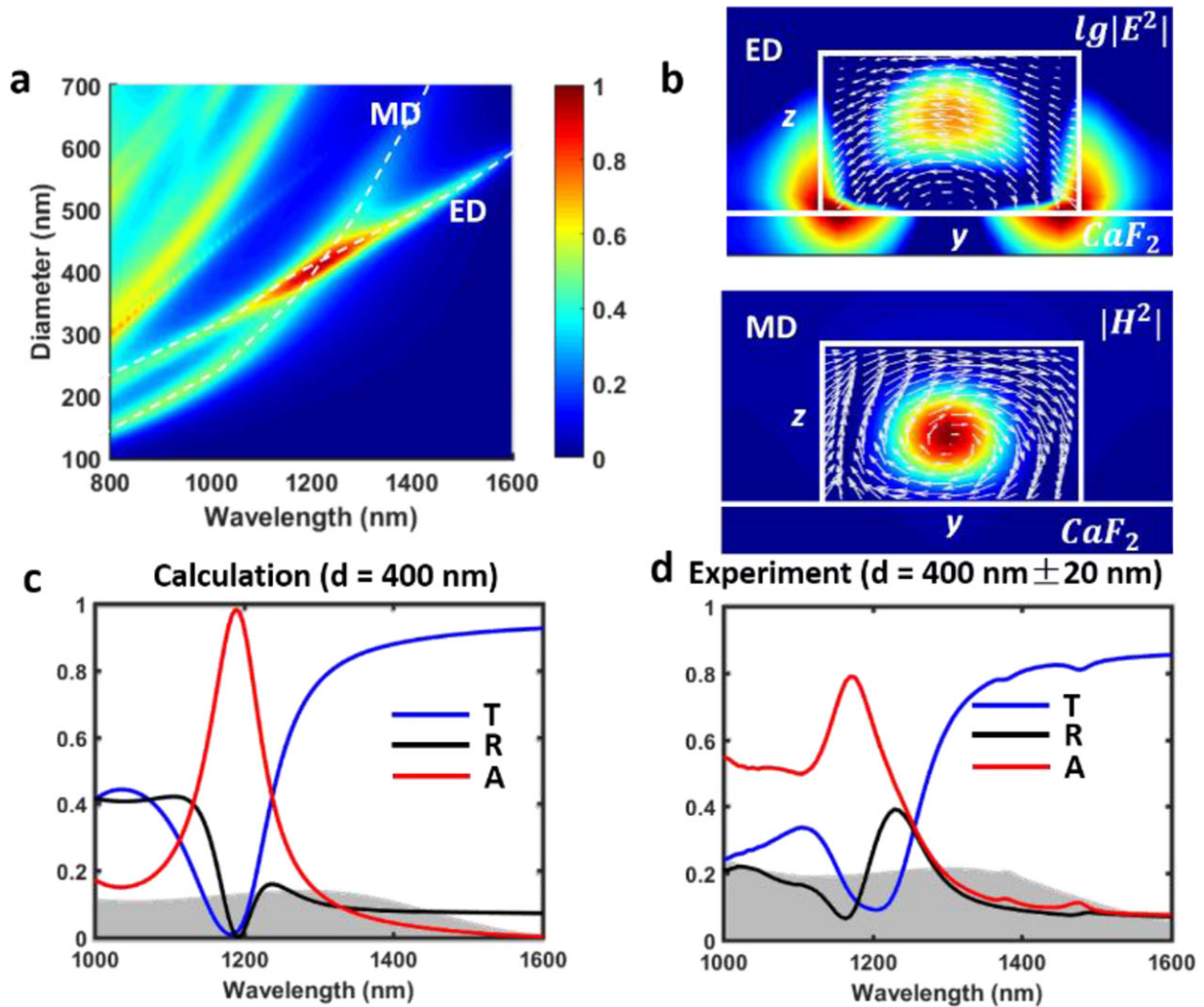


**Figure 4.** Absorption spectra of the Ge metasurface absorber on the  $\text{CaF}_2$  substrate under normal illumination. a) Calculated absorption spectra while the diameter  $d$  is varied from 100 nm to 700 nm. The white dashed lines highlight the enhanced absorption at each resonance (ED and MD). b) The corresponding field distribution in the  $yz$ -plane inside each disk near the ED and MD resonances. The arrows denote corresponding electric field vectors. c) Calculated and d) experimental transmission, reflection, and absorption spectra at  $d = 400$  nm. The shadows denote the absorption spectra of a 160 nm-thin Ge film on the substrate.

direction ( $T = |t|^2 = 0$ ), which is equivalent to achieving complete destructive interference between the scattered field and the incident field within each period, the only requirement is that  $P_{\text{scat},z} = P_0$  in each period (III in Figure 2), or  $P_{\text{scat},z}/I_0 = a^2$ . Here,  $P_{\text{scat},z}$  denotes the forward scattered power of an individual disk along  $z$ -direction,  $P_0$  denotes the incident power within each period,  $I_0$  corresponds to the source intensity, and  $P_{\text{scat},z}/I_0$  represents the forward scattering cross section of a single Ge disk. By optimizing  $a$  according to this relation, the forward scattering cross section of each disk equals to the physical cross section of each period at the crossing region of ED and MD. This enables complete destructive interference between the scattered field and the incident field in the forward direction ( $T = 0$ ). Perfect absorption ( $A = 1 - T - R = 100\%$ ) can thus be achieved.

Multipole decompositions of the scattering behavior of a single Ge disk<sup>[51–56]</sup> are conducted in vacuum (See Supporting Information for details of conducting multipole decompositions). Its

total scattering cross section can be decomposed into the contributions from the electric dipole (ED), the magnetic dipole (MD), the electric quadrupole (EQ), and the magnetic quadrupole (MQ), as shown in Figure 3a. The thickness  $h$  and the diameter  $d$  of the Ge disk here are chosen to be  $h = 160$  nm and  $d = 400$  nm in Figure 3a, making the ED resonance and MD resonance spectrally overlap and oscillate in phase with each other near 1200 nm wavelength. Contributions from higher-order multipoles can be neglected in this spectrum region. The radiation pattern near the wavelength of 1200 nm in the inset further validates that Kerker Condition is fulfilled.

In Figure 3b,  $a$  is set to be  $a \approx 650$  nm, that is,  $g = d - a \approx 250$  nm. Then, the forward scattering cross section of each disk (denoted by the black line) equals the physical cross section of each period,  $a^2$  (denoted by the red dashed line) near 1200 nm.

To prove the validity of our analysis, the absorption spectra of a Ge metasurface absorber with  $h = 160$  nm as the function

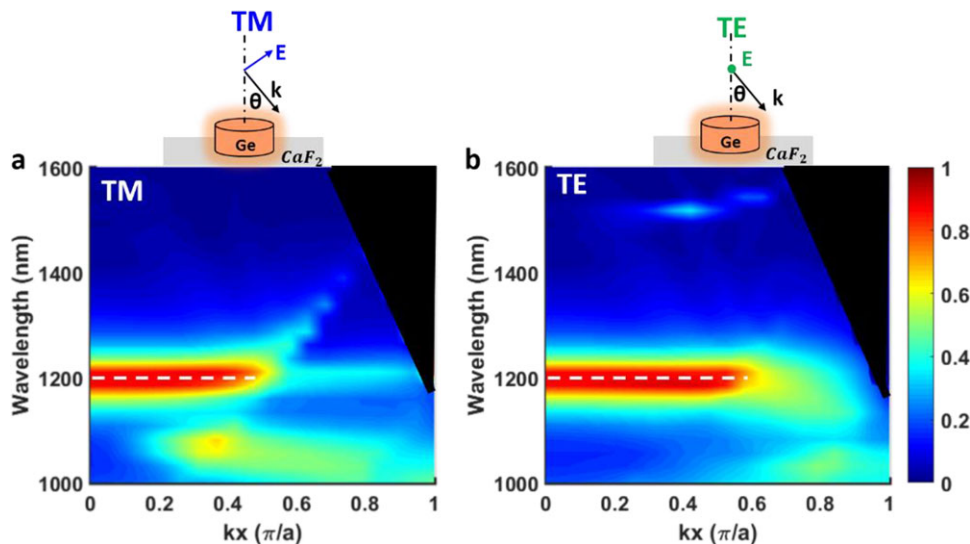


**Figure 5.** Absorption spectra of a Ge metasurface absorber with  $d = 400$  nm,  $h = 160$  nm, and  $a = 650$  nm on a  $\text{CaF}_2$  substrate, as a functions of in-plane wave vector  $k_x$  (normalized by  $\pi/a$ ) for different polarizations. Calculated absorption spectra under a) TM and b) TE illuminations.  $k_x = (2\pi/\lambda) \sin\theta$ . The dark regions correspond to  $k_x > k_0$ .

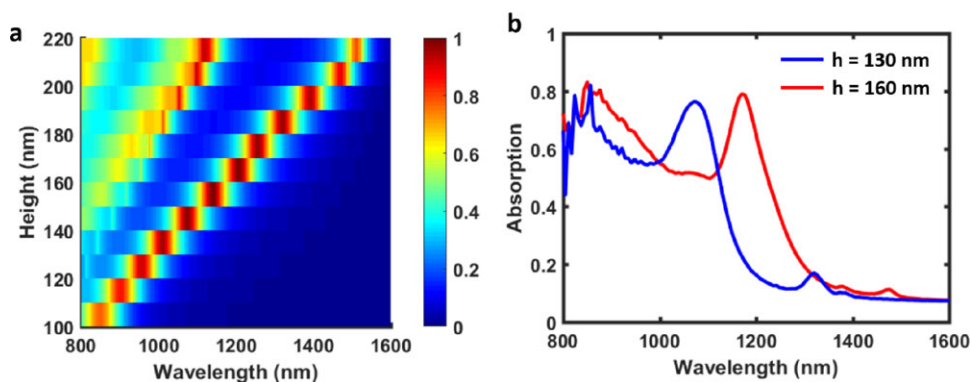


**Figure 6.** Wide-band tunability of the all-dielectric metasurface absorber consisting of Ge disks with different heights on the  $\text{CaF}_2$  substrate in the near infrared region. a) Calculated absorption of the all-dielectric metasurface absorber consisting of Ge disks with the height varying from 100 nm to 220 nm with a step size of 10 nm at fixed gap size ( $g = 250$  nm), where the diameter is adjusted ( $d/h \approx 2.5$ ) so that MD and ED overlap with each other at each height in the near-infrared region. b) Experimental illustration of the absorption spectra of the all-dielectric metasurface absorber consisting of Ge disks with two different heights (130 and 160 nm).

of the diameter  $d$  and wavelength are shown in **Figure 4a**. The white dashed lines highlight the enhanced absorption at each resonance (ED and MD) and denote their relative spectral shift under different aspect ratios ( $d/h$ ). The corresponding field distributions in the  $yz$ -plane inside each disk are shown in **Figure 4b**. For each single resonance, the absorption of the metasurface can never exceed 50%. While the absorption can easily approach 100% at the crossing region of the ED and MD near 1200 nm when  $d = 400$  nm.

Both transmission and reflection are suppressed near 1200 nm, as shown in **Figure 4c**. The performance of this metasurface is also investigated in the experiment, as illustrated in **Figure 4d**, with about 80% absorption near 1200 nm. The discrepancies between the simulation and experiment are mainly from the error of nanofabrication techniques. The method we used to deposit germanium film is thermal evaporation, which shows the weakness of leaving scarifications on the deposited

film. Therefore, the performance of the metasurface degrades at the maximum absorption near the wavelength of 1200 nm. Moreover, the optical response at shorter wavelength is more sensitive to the shape of nanoantennas and film quality (e.g., more scattering due to scarifications on the surface of the film), which results in the deviation of the experimental absorption spectrum from the simulation below the wavelength of 1100 nm.

In comparison, the absorption spectrum of a 160 nm thin Ge film on the same  $\text{CaF}_2$  substrate is also denoted by grey shadows in **Figure 4c,d**, where the absorption barely reaches 20% near the wavelength of 1200 nm.

The dependence of the absorption of such an all-dielectric metasurface absorber on the incident polarization and angle is also studied. In **Figure 5a,b**, the absorption spectra as a function of incident angle under TM and TE illuminations are calculated. The absorption at 1200 nm wavelength is almost polarization-insensitive. The high absorption ( $>80\%$ ) originating from the

overlapped ED and MD near 1200 nm can be maintained within 28° range ( $k_x < 0.5\pi/a$ ) for both polarizations, highlighted by the white dashed lines in Figure 5a,b. The dark regions represent the condition when  $k_x > k_0$ .

Moreover, considering that Ge has little dispersion in the near-infrared region, the crossing of MD and ED ( $R = 0$ ) can be achieved through a fixed aspect ratio ( $d/h \approx 2.5$ ), when  $h$  varies from 100 nm to 220 nm. In Figure 6a, the near-unity absorption (>70%) can be tailored throughout the near infrared region (800–1600 nm) with fixed aspect ratio and gap size ( $g = 250$  nm), which means that the high absorption shows high tolerance to the gap size. For each thickness, the performance of the all-dielectric metasurface absorber can be further optimized by using specific  $a$  (or  $g$ ) to completely cancel the forward emission ( $T = 0$ ). In Figure 6b, the high absorption (>70%) of the all-dielectric metasurface absorber consisting of Ge disks with  $h = 130$  nm or  $h = 160$  nm is illustrated experimentally, which is in good accordance with our calculation in Figure 6a.

#### 4. Conclusions and Outlook

In conclusion, an all-dielectric Ge metasurface absorber in the near-infrared region is both theoretically and experimentally demonstrated. It was shown that near-unity absorption can be achieved in such subwavelength-thin structures without the aid of back reflector due to the destructive interference between simultaneously excited electric dipoles and magnetic dipoles inside each element in the backward direction along with the destructive interference between the scattered field and the incident field in the forward direction. This absorption is much higher than the theoretical maximum absorption of a free-standing ultrathin film. And it is polarization-independent and angle-insensitive, with over 80% absorption at an incident angle up to 28°. By adjusting the geometric parameters of the element in the metasurface, its high absorption performance can be tailored throughout the near infrared region (800–1600 nm). This all-dielectric metasurface absorber is ultrathin and flexible, making it a good candidate for high-speed and high-efficiency optoelectronic devices aimed for photodetecting and energy harvesting.

#### Acknowledgements

J.T. and H.L. contributed equally to this work. This work is supported by National Key Research and Development Program of China (2017YFA0205700 and 2017YFE0100200) and National Natural Science Foundation of China (Grant Nos. 61425023, 61575177, 61775194).

#### Conflict of Interest

The authors declare no conflict of interest.

#### Keywords

all-dielectric metasurfaces, germanium nanostructures, near-infrared, perfect absorption, single-layer

- [1] L. Colace, G. Assanto, *IEEE Photonics J.* **2009**, *1*, 69.
- [2] R. Kaufmann, G. Isella, A. Sanchez-Amores, S. Neukom, A. Neels, L. Neumann, A. Brenzikofer, A. Dommann, C. Urban, H. von Känel, *J. Appl. Phys.* **2011**, *110*, 023107.
- [3] N. T. Tung, T. Tanaka, *Phot. Nano. Fund. Appl.* **2018**, *28*, 100.
- [4] L. Tang, S. E. Kocabas, S. Latif, A. K. Okyay, D.-S. Ly-Gagnon, K. C. Saraswat, D. A. B. Miller, *Nat. Photon.* **2008**, *2*, 226.
- [5] J. Michel, J. Liu, L. C. Kimerling, *Nat. Photon.* **2010**, *4*, 527.
- [6] C. Rouse, J. W. Zeller, H. Efstathiadis, P. Haldar, J. S. Lewis, N. K. Dhar, P. Wijewarnasuriya, Y. R. Puri, A. K. Sood, *Opt. Photonics J.* **2016**, *06*, 61.
- [7] P. Nagpal, S. E. Han, A. Stein, and D. J. Norris, *Nano. Lett.* **2008**, *8*, 3238.
- [8] H. A. Atwater, A. Polman, *Nat. Mater.* **2010**, *9*, 205.
- [9] D. M. Bierman, A. Lenert, W. R. Chan, B. Bhatia, I. Celanović, M. Soljačić, E. N. Wang, *Nat. Energy* **2016**, *1*, 16068.
- [10] S. J. Kim, J. Park, M. Esfandyarpour, E. F. Pecora, P. G. Kik, M. L. Brongersma, *Nano. Lett.* **2016**, *16*, 3801.
- [11] Z. Li, S. Butun, K. Aydin, *ACS Nano* **2014**, *8*, 8242.
- [12] K. Aydin, V. E. Ferry, R.M. Briggs, H. A. Atwater, *Nat Commun* **2011**, *2*, 517.
- [13] X. Fang, M.L. Tseng, D.P. Tsai, Nikolay I. Zheludev, *Phys. Rev. A* **2016**, *5*, 014010.
- [14] P.-C. Wu, C.-Y. Liao, J.-W. Chen, D.P. Tsai, *Adv. Opt. Mater* **2017**, *5*, 1600581.
- [15] N. Liu, M. Mesch, T. Weiss, H. Giessen, *Nano Lett.* **2010**, *10*, 2342.
- [16] W. Wang, Y. Qu, K. Du, S. Bai, J. Tian, M. Pan, H. Ye, M. Qiu, Q. Li, *Appl. Phys. Lett.* **2017**, *110*, 101101.
- [17] Y. Qu, Q. Li, K. Du, L. Cai, J. Lu, M. Qiu, *Laser Photonics Rev.* **2017**, *11*, 1700091.
- [18] C. M. Watts, X. Liu, W. J. Padilla, *Adv. Mater.* **2012**, *24*, OP98.
- [19] X. Chen, H. Gong, S. Dai, D. Zhao, Y. Yang, Q. Li, M. Qiu, *Opt. Lett.* **2013**, *38*, 2247.
- [20] S. Dai, D. Zhao, Q. Li, M. Qiu, *Opt. Express* **2013**, *21*, 013125.
- [21] Y. Chen, X. Li, X. Luo, S. A. Maier, M. Hong, *Photonics Res.* **2015**, *3*, 54.
- [22] M. A. Kats, R. Blanchard, P. Genevet, F. Capasso, *Nat. Mater.* **2013**, *12*, 20.
- [23] Y. Qu, Q. Li, H. Gong, K. Du, S. Bai, D. Zhao, H. Ye, M. Qiu, *Adv. Opt. Mater.* **2016**, *4*, 480.
- [24] K. Du, Q. Li, Y. Lyu, J. Ding, Y. Lu, Z. Cheng, M. Qiu, *Light: Sci. Appl.* **2017**, *6*: e16194.
- [25] K. Du, L. Cai, H. Luo, Y. Lu, J. Tian, Y. Qu, P. Ghosh, Y. Lyu, Z. Cheng, M. Qiu, Q. Li, *Nanoscale* **2018**, *10*, 4415.
- [26] L. Cai, K. Du, Y. Qu, H. Luo, M. Pan, M. Qiu, Q. Li, *Opt. Lett.* **2018**, *43*, 1295.
- [27] Y. Qu, Q. Li, L. Cai, M. Pan, P. Ghosh, K. Du, M. Qiu, *Light: Science & Applications* **2018**, *7*, 26.
- [28] P. C. Wu, C. Y. Liao, V. Savinov, T. L. Chung, W. T. Chen, Y.-W. Huang, P. R. Wu, Y.-H. Chen, A.-Q. Liu, N. I. Zheludev, D. P. Tsai, *ACS nano* **2018**, *12*, 1920.
- [29] V. S. Asadchy, I. A. Faniayeu, Y. Ra'di, S. A. Khakhomov, I. V. Semchenko, S. A. Tretyakov, *Phys. Rev. X* **2015**, *5*, 031005.
- [30] J. C. Ginn, I. Brener, D. W. Peters, J. R. Wendt, J. O. Stevens, P. F. Hines, L. I. Basilio, L. K. Warne, J. F. Ihlefeld, P. G. Clem, M. B. Sinclair, *Phys. Rev. Lett.* **2012**, *108*, 097402.
- [31] C.H. Chu, M.L. Tseng, J. Chen, P.C. Wu, Y. Chen, H.C. Wang, T.Y. Chen, W.T. Hsieh, H.J. Wu, G. Sun, D.P. Tsai, *Laser Photonics Rev.* **2016**, *10*, 1063.

- [32] S. Jahani, Z. Jacob, *Nat Nano* **2016**, *11*, 23.
- [33] H.-C. Wang, C.H. Chu, P.C. Wu, H.-H. Hsiao, H.J. Wu, J.-W. Chen, W.H. Lee, Y.-C. Lai, Y.-W. Huang, M.L. Tseng, S.-W. Chang, D.P. Tsai, *Small* **2018**, *14*, 1703920.
- [34] G. P. Zograf, M. I. Petrov, D. A. Zuev, P. A. Dmitriev, V. A. Milichko, S. V. Makarov, P. A. Belov, *Nano Lett.* **2017**, *17*, 2945.
- [35] A. E. Miroshnichenko, M. I. Tribelsky, *Phys. Rev. Lett.* **2018**, *120*, 033902.
- [36] J. R. Piper, V. Liu, S. Fan, *Appl. Phys. Lett.* **2014**, *104*.
- [37] M. A. Cole, D. A. Powell, I. V. Shadrivov, *Nanotechnology* **2016**, *27*, 424003.
- [38] X. Liu, K. Fan, I. V. Shadrivov, W. J. Padilla, *Opt. Express* **2017**, *25*, 191.
- [39] K. Fan, J. Y. Suen, X. Liu, W. J. Padilla, *Optica* **2017**, *4*, 601.
- [40] E. D. Palik, *Handbook of Optical Constants of Solids* **1998**, Vol. 3, Academic Press, San Diego.
- [41] A. B. Evlyukhin, S. M. Novikov, U. Zywietz, R. L. Eriksen, C. Reinhardt, S. I. Bozhevolnyi, B. N. Chichkov, *Nano Lett.* **2012**, *12*, 3749.
- [42] A. E. Krasnok, A. E. Miroshnichenko, P. A. Belov, Y. S. Kivshar, *Opt. express* **2012**, *20*, 20599.
- [43] J. M. Geffrin, B. Garcia-Camara, R. Gomez-Medina, P. Albella, L. S. Froufe-Perez, C. Eyraud, A. Litman, R. Vaillon, F. Gonzalez, M. Nieto-Vesperinas, J. J. Saenz, F. Moreno, *Nat. Commun.* **2012**, *3*, 1171.
- [44] I. Staude, A. E. Miroshnichenko, M. Decker, N. T. Fofang, S. Liu, E. Gonzales, J. Dominguez, T. S. Luk, D. N. Neshev, I. Brener, *ACS Nano* **2013**, *7*, 7824.
- [45] J. Yan, P. Liu, Z. Lin, H. Wang, H. Chen, C. Wang, G. Yang, *ACS Nano* **2015**, *9*, 2968.
- [46] P. Spinelli, M. A. Verschuuren, A. Polman, *Nat. Commun.* **2012**, *3*, 692.
- [47] M. Decker, I. Staude, M. Falkner, J. Dominguez, D. N. Neshev, I. Brener, T. Pertsch, Y. S. Kivshar, *Adv. Opt. Mater.* **2015**, *3*, 813.
- [48] Y. F. Yu, A. Y. Zhu, R. Paniagua-Dominguez, Y. H. Fu, B. Luk'yanchuk, A. I. Kuznetsov, *Laser Photonics Rev.* **2015**, *9* (4), 412.
- [49] M. I. Tribelsky, J.-M. Geffrin, A. Litman, C. Eyraud, F. Moreno, *Sci. Rep.* **2015**, *5*, 12288.
- [50] W. Liu, Y. S. Kivshar, *Opt. Express* **2018**, *26*, 13085.
- [51] A. B. Evlyukhin, C. Reinhardt, B. N. Chichkov, *Phys. Rev. B: Condens. Matter* **2011**, *84*, 235429.
- [52] D. Sikdar, W. Cheng, M. Premaratne, *J. Appl. Phys.* **2015**, *117*, 083101.
- [53] J. Tian, Q. Li, Y. Yang, M. Qiu, *Nanoscale* **2016**, *8*, 4047.
- [54] J. Tian, Y. Yang, M. Qiu, F. Laurell, V. Pasiskevicius, H. Jang, *Opt. Express* **2017**, *25*, 24068.
- [55] Y. Yang, A. E. Miroshnichenko, S. V. Kostinski, M. Odit, P. Kapitanova, M. Qiu, Y. S. Kivshar, *Phys. Rev. B* **2017**, *95*, 165426.
- [56] A. E. Miroshnichenko, A. B. Evlyukhin, Y. S. Kivshar, B. N. Chichkov, *ACS Photonics* **2015**, *2*, 1423.